ADVANCED FUNCTIONAL MATERIALS
www.afm-journal.de

Transient Stiffness Patterning in Hydrogels Driven by Dissipative Mechanochemical Coupling

*Roberto Baretta, Maria F. Pantano, and Marco Frasconi**

Living systems adapt to mechanical forces through a series of biochemical feedback loops and dissipative signal transduction mechanisms across multiple length scales. By contrast, synthetic materials are static, closed systems with minimal interaction with their surroundings and lack the ability to adapt to mechanical deformations. Here, a strategy that enables a hydrogel to adapt to mechanical forces through the temporal modulation of its stiffness properties is reported. It is demonstrated that force-induced bond rupture at the disulfide linkages of the hydrogel, coupled with their chemical reoxidation leads to dissipative, transient stiffness functions. The electrochemical generation of the oxidant as the output of a feedback loop triggered by an externally applied force provides high spatiotemporal control over the dissipative process, enabling the engineering of hydrogels with out-of-equilibrium stiffness patterns. Additionally, dose-controlled, spatiotemporal transient release of model protein payloads from the hydrogel is demonstrated. The proposed concept has the potential to enhance the autonomous and interactive functionalities of hydrogels, advancing their applications in the biomedical field and soft robotics.

1. Introduction

The dynamic interplay between mechanical and biochemical processes endows living systems with robustness and adaptability, enabling them to maintain structural integrity while interacting with the environment.[1,2] For example, cells exhibit remarkable sensitivity to external mechanical stimuli, triggering a cascade of biochemical responses[3] that allow them to adapt to their surroundings through feedback regulation. This mechanotransduction process is essential for stem cell differentiation, directing cellular remodeling in response to changes in the stiffness of the extracellular matrix (ECM).[4] Furthermore, the coupling between mechanical and biochemical events drives the formation of spatiotemporal cellular patterns within tissues,[5] leading to the emergence of structures that support their specific functions. These are intrinsically nonequilibrium processes, with mechano-chemical dissipative couplings occurring in both directions to enable functional adaptation.

Synthetic materials that mimic the adaptive processes of living systems have been developed through the self-assembly of diverse building blocks under dissipative conditions, enabling control over the lifetime and properties of the assembled structures through the consumption of chemical fuels.[6–8] Hydrogels with transient mechanical properties, powered by chemical[9,10] or enzymatic[11,12] reactions, electricity,[13] or light,[14–16] can execute complex operations, such as autonomous mechanical actuation.[16–18] Despite recent progress, dissipative materials that use force-controlled deformations as an energy source to activate and regulate their responses autonomously, mimicking the mechanotransduction process, remain largely unexplored. Indeed, mechanical forces are widely recognized in polymer mechanochemistry as a powerful tool for triggering chemical reactions, enabling precise tuning of the properties of polymeric materials.[19,20] In this context, significant progress has been made in developing self-strengthening polymers capable of increasing both mass and strength under mechanical stress.[21,22] However, the development of mechanically adaptive materials regulated by chemical feedbacks is often unconcerned in this research field despite their potential to enable more autonomous and interactive functionalities that can find a wide range of applications, from biomedical devices[23] to soft robotics.[24]

Here, we demonstrate how a mechano-responsive hydrogel can achieve temporal modulation of its stiffness as an adaptive response to force-driven deformation. Our strategy for designing the bioinspired mechano-chemical dissipative materials is illustrated in **Figure 1**.

In this system, the disulfide linkages in the hydrogel network, being mechanochemically responsive,[25,26] undergo homolytic cleavage under compressive stress, generating radicals that

R. Baretta, M. Frasconi
Department of Chemical Sciences
University of Padova
Via Marzolo 1, Padova 35131, Italy
E-mail: marco.frasconi@unipd.it
M. F. Pantano
Department of Civil, Environmental and Mechanical Engineering
University of Trento
Via Mesiano 77, Trento 38123, Italy

The ORCID identification number(s) for the author(s) of this article can be found under https://doi.org/10.1002/adfm.202502531

DOI: 10.1002/adfm.202502531

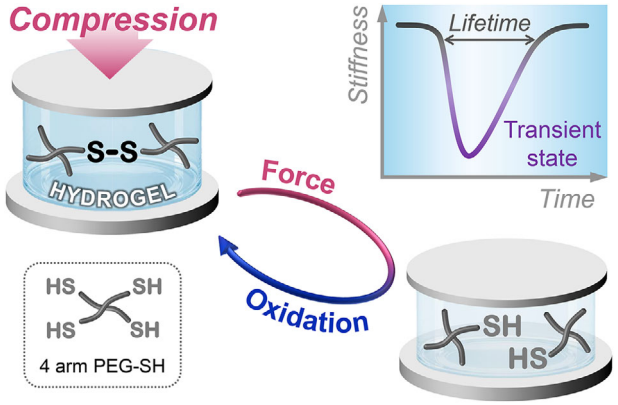

Figure 1. Schematic illustration of the dissipative mechanochemical coupling in hydrogels. Hydrogel adapts to mechanical stress that induces bond rupture at the disulfide linkages through chemical or electrochemical reoxidation, resulting in transient stiffness changes.

abstract hydrogens from water to form thiols,[27–29] thereby weakening the overall hydrogel structure. The concurrent oxidation of thiols into disulfides, driven by chemical or electrochemically generated oxidants, results in the transient modulation of the stiffness properties of the hydrogel, enabling an adaptive response to the mechanical deformation. The high spatiotemporal control achieved through this mechano-electrochemical dissipative process allowed us to generate temporally controlled stiffness patterns on the hydrogel. We also demonstrate the dose-controlled, transient release of a model protein payload from the hydrogel induced by external forces coupled with an enzymatically driven reaction.

2. Results and Discussion

2.1. Mechano-Chemical Dissipative Hydrogel

Disulfide-crosslinked hydrogels were prepared from thiol terminated 4-arm-poly(ethylene glycol) (4-arm-PEG-SH, MW 5000), chosen for their easily tunable mechanical properties and broad technological applicability. Disk-shaped hydrogels were obtained by oxidizing 4-arm-PEG-SH (5% w/v) with an Fe^{3+}-ethylenediaminetetraacetic acid complex in 0.1 M phosphate-buffered saline (PBS) at pH 7.4. The resulting hydrogel exhibited a characteristic "J-shaped" stress-strain curve, as determined by dynamic mechanical analysis (DMA), with an initial linear response (**Figure** 2A; Figure S1, Supporting Information). The hydrogel failed at ≈ 51.6 ± 2.8% strain and had a compressive modulus of 12.8 ± 2.6 kPa, consistent with values reported for other disulfide-crosslinked 4-arm PEG hydrogels.[13,27,30] The formation of thiols resulting from the cleavage of disulfide crosslinkers under compressive stress was monitored using confocal laser microscopy after treatment of the compressed hydrogel with fluorescein isothiocyanate (FITC), which rapidly reacts with aliphatic thiols to form stable dithiourethane adducts.[31,32] Various weights were applied to the gel disks, producing compressive stresses ranging from 2.0 to 9.8 kPa, calculated as the ratio of the applied force to the contact area of the hydrogel. The fluorescence intensity of the hydrogels after treatment with FITC increased progressively with higher compressive stresses (Figure 2B; Figure S2, Supporting Information) and longer compression times (Figure S3, Supporting Information), indicating the formation of larger amounts of thiols. To demonstrate the reversibility of disulfide bond rupture induced by mechanical stress, the compressed hydrogels were immersed in a 10 mM hydrogen peroxide (H_2O_2) solution for 8 hours, followed by thorough washing and subsequent treatment with FITC. No fluorescence was detected in the hydrogels subjected to compressive stresses up to 5.9 kPa after hydrogen peroxide treatment, indicating that disulfide bonds were reformed within the hydrogel network through H_2O_2-mediated oxidation of thiols. Only the hydrogels subjected to 9.8 kPa exhibited residual fluorescence, suggesting incomplete restoration of the disulfide-crosslinked network within the reaction time, due to the large extent of disulfide bond rupture. This observation is further supported by the cyclic compressive stress-strain curves (Figure S1B, Supporting Information), which show a noticeable hysteresis loop under high stress.

The reversible disulfide rupture and reformation process for compressive stresses up to 5.9 kPa allow us to investigate the hydrogel's mechanical properties within a mechano-chemical dissipative framework, where the mechanical force weakens the network, and concurrent chemical oxidation drives linkages reformation. As shown in Figure 2C, the hydrogel subjected to a compressive stress of 3.9 kPa for 1 h in the presence of 10 mM H_2O_2 exhibits an initial decrease in stiffness (measured as G' by rheometry) due to disulfide bond rupture, which weakens the hydrogel network. Upon release of the compressive deformation, the stiffness of the hydrogel increases, returning to its original value. The minimum stiffness (G'_{min}) and the lifetime of the softened hydrogel depend on the applied compression. Increasing the compressive stress from 2.0 to 5.9 kPa in the presence of 10 mM H_2O_2 reduces G'_{min} from 250 to 160 Pa. Upon release of the compressive deformation, the stiffness of the hydrogel increases, returning to its original value within 3 h for the hydrogel subjected to 2.0 kPa stress and extending to 7 h for a compression of 5.9 kPa. This effect is attributed to the rupture of larger amounts of disulfide bonds at higher stress levels. No significant change in G′ (G′ ≈ 300 Pa) was observed for the hydrogel in 10 mM H_2O_2 without compression.

Interestingly, the transient softening of the hydrogel can be modulated by the H_2O_2 concentration: a higher concentration (25 mM) results in smaller stiffness variations and shorter lifetimes, while a lower concentration (2.5 mM) leads to much larger stiffness variations and extended lifetimes (Figure 2D). This experimental evidence indicates that higher H_2O_2 concentrations restore the disulfide-crosslinked hydrogel network more rapidly. In contrast, in the absence of H_2O_2, applying the same compressive stress to the hydrogel reduces its stiffness to lower G'_{min} (Figure 2D, gray curve), and the stiffness gradually decreases even after the compressive load is removed. Thus, thiol reoxidation by H_2O_2 is essential to restore the original, high-stiffness state of the hydrogel after mechanical deformation, resulting in a mechanochemical dissipative material displaying transient stiffness properties.

The compression-induced transient softening process in the presence of H_2O_2 is reversible and does not compromise the overall stability of the hydrogel network. This feature was demonstrated by applying repeated compressive stress cycles

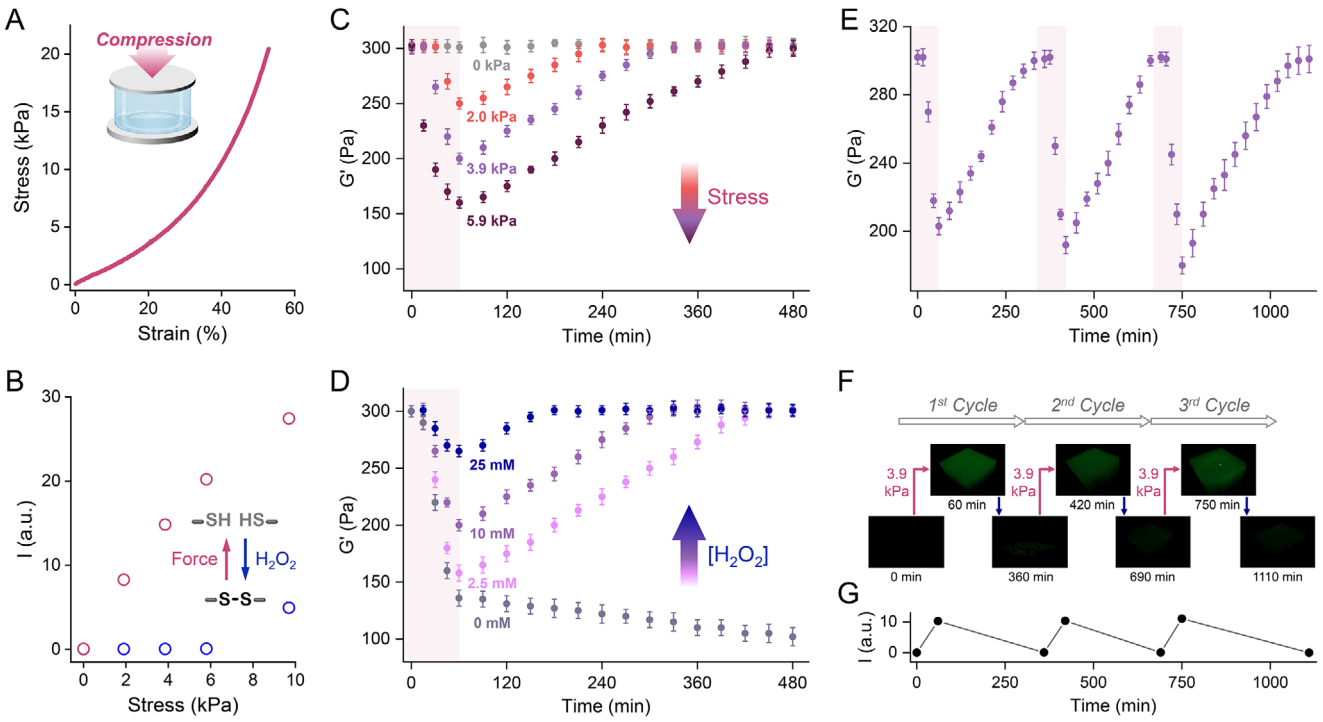

Figure 2. Mechano-chemical control of the transient stiffness properties of the hydrogel. A) Example compression stress-strain curve of the hydrogel. B) Fluorescence intensity (I) of the hydrogel subjected to various compressive stress for 1 h (red circles) and after subsequent immersion for 8 h in a 10 mM H_2O_2 solution in PBS 0.1 M at pH 7.4 (blue circles). C) Temporal changes in hydrogel stiffness (G′) in a 10 mM H_2O_2 solution in PBS 0.1 M at pH 7.4, subjected to different compressive stress for 1 h (kPa): 0, 2.0, 3.9 and 5.9. D) Temporal changes in hydrogel stiffness (G′) subjected to 3.9 kPa compressive stress for 1 h in the presence of H_2O_2 solutions (0.1 M PBS, pH 7.4) at different concentrations (mM): 0, 2.5, 10, and 25. E) Temporal changes in hydrogel stiffness (G′) under compressive loading cycles (3.9 kPa, 1 h) in a 10 mM H_2O_2 solution. F) Laser scanning confocal microscope images of hydrogels in a 10 mM H_2O_2 solution, collected during consecutive compressive cycles at 3.9 kPa for 1 h and following stress removal, and (G) corresponding fluorescence intensity (I) of the hydrogel over three cycles.

to the same hydrogel sample, which exhibited consistent stiffness changes and lifetimes over three full cycles (Figure 2E). The stability of the hydrogel was further confirmed by confocal microscopy using independent hydrogel samples, each treated with FITC after either a compressive cycle or subsequent stress removal. Confocal microscopy images displayed similar fluorescence intensities at the minimum stiffness for each compression cycle, indicating consistent thiol generation during repetitive compressions (Figure 2F). Additionally, the absence of fluorescence at the end of each dissipative cycle indicates the complete restoration of the disulfide-crosslinked network by H_2O_2. These results demonstrate that our disulfide-crosslinked hydrogel can adapt to varying mechanical loading conditions by exhibiting transient stiffness properties through bond rupture, and can autonomously recover to its original high-stiffness state in the presence of a chemical oxidant.

2.2. Spatiotemporal Hydrogel Softening Driven by Mechano-Electrochemical Dissipation

Oxidizing agents for disulfide re-formation can also be generated electrochemically,[13,33] providing a clean energy source with minimal chemical waste and offering spatiotemporal modulation. Indeed, the use of electrochemical energy to drive the assembly and operations of materials far from equilibrium has recently attracted growing attention.[13,34,35] Since the electrogeneration of reactive species is diffusion-controlled from the electrode surface, reactant gradients can be generated and shaped by the electrode's geometry.[36] For example, spatially controlled electrochemical inputs were employed to precisely localize gelation, enabling reversible, reprogrammable, and 3D patterning for various applications, including information storage.[37,38] Here, we investigated the temporal stiffness changes in the hydrogel induced by an applied deformation coupled with an electrochemically generated oxidant. Toward this end, we used ferrocene as an efficient, regenerable electrocatalyst for the electrochemically mediated oxidation of thiols to disulfides.[13] As schematically outlined in **Figure 3A**, the hydrogel disk was placed on a planar screen-printed electrode comprising a glassy carbon working electrode, an Ag/AgCl paste reference electrode, and a carbon counter electrode. The hydrogel was then soaked in an 8 mM ferrocenecarboxylic acid (Fc) solution in 0.1 M PBS (pH 7.4) and remained in the same solution throughout the experiment. Cyclic voltammetric experiments on the hydrogel-modified electrode showed the reversible oxidation of Fc at 0.344 V and the reduction of Fc^+ at 0.229 V (Figure S4, Supporting Information). A constant oxidative voltage (E) of 1.0 V was then applied to the electrode to continuously generate Fc^+, while the hydrogel was

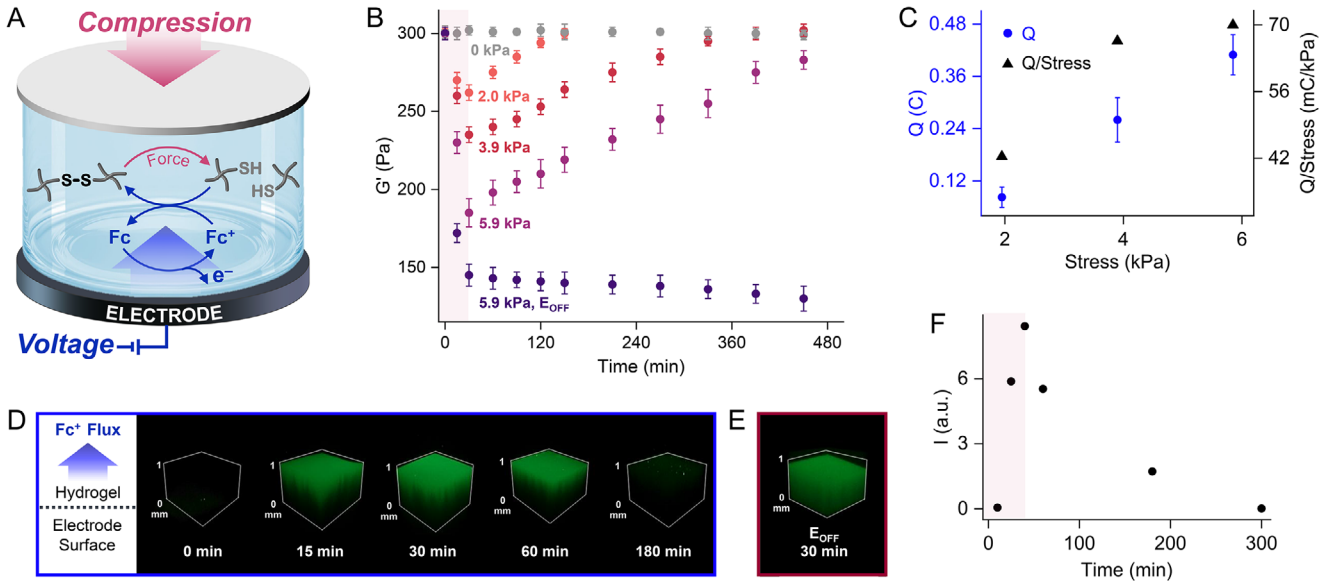

Figure 3. Mechano-electrochemical dissipative hydrogel. A) Schematic representation of transient hydrogel softening induced by mechanical deformation and re-oxidation of disulfide crosslinkers mediated by Fc^+, electrochemically generated at the electrode under a constant voltage. B) Temporal changes in hydrogel stiffness (G′) under continuous 1.0 V application in 8 mM Fc solution, subjected to 30 min compressive stress (kPa): 0, 2.0, 3.9 and 5.9. Purple curve represents the G' values of the hydrogel subjected to 5.9 kPa compressive stress for 30 min in the absence of applied voltage (E_{OFF}). C) Oxidative charge (Q, blue circles), as determined by chronoamperometry, and Q normalized per stress unit (black triangles) for the transient stiffness process under different compressive stresses. D) Confocal microscopy images of hydrogels in 8 mM Fc solution subjected to 3.9 kPa compressive stress for 30 min under continuous voltage application. E) Confocal image of the hydrogel subjected to 3.9 kPa compressive stress for 30 min without voltage application. F) Fluorescence intensity (I) of the corresponding confocal microscopy images displayed in (D).

compressed. The stiffness properties of the hydrogel were monitored by rheometry, as illustrated in Figure 3B.

Applying increasing compressive stresses of 2.0, 3.9, and 5.9 kPa to the hydrogel for 30 min under continuous voltage application led to a progressive decrease in stiffness, from an initial value of 300 Pa to G'_{min} values of 260, 230, and 185 Pa, respectively. This decrease is consistent with network weakening due to compression-induced disulfide bond rupture. Following compression removal, the stiffness of the hydrogel gradually increased, returning to its initial high value within ≈ 2, 5, and 8 h for initial stresses of 2.0, 3.9, and 5.9 kPa, respectively. This demonstrates that thiols in the hydrogel are re-oxidized by Fc^+ generated at the electrode, restoring the disulfide crosslinkers within the network. As a control, no changes in stiffness were observed in the hydrogel when voltage was applied without compression. Conversely, without applied voltage, the hydrogel subjected to 5.9 kPa stress failed to recover its high-stiffness state, with G' remaining at 140 Pa after compression. This confirms that electrogenerated Fc^+ mediates the re-oxidation of thiols to disulfide.

The oxidative charge (Q) required to restore the high-stiffness state of the hydrogel, determined from the integration of the chronoamperometric curves recorded during the transient softening process (Figure S5, Supporting Information), increases with higher compressive stress (Figure 3C). Since the oxidative charge reflects the extent of disulfide bond reformation, this trend indicates that greater amounts of Fc^+ must be electrogenerated to re-oxidize the larger amounts of thiols formed under higher compressive stress. Furthermore, normalizing the oxidative charge to the compressive stress reveals an increase in the Q/stress ratio from 43 mC kPa^{-1} for the hydrogel subjected to 2.0 kPa compressive stress to ≈ 70 mC kPa^{-1} at 3.9 and 5.9 kPa. This indicates that at higher compressive stresses more charge per unit of stress is required to restore the hydrogel network. The rise of the Q/stress ratio at higher stresses suggests a decrease in the efficiency of disulfide bond reformation by the applied voltage, likely due to more extensive network disruption. This trend can also be interpreted as a measure of the hydrogel's adaptability to mechanical deformation: at lower stress, the network responds more efficiently and requires less oxidative charge for recovery, whereas, at higher stress, the extended network deformation demands increased oxidative charge to achieve re-crosslinking and network restoration.

The formation of thiols in the hydrogel network during the mechano-electrochemically driven transient softening was confirmed by laser confocal microscopy. During 30 min of compressive stress, a progressive increase in fluorescence was observed (Figure 3D,F), indicating thiol formation in the compressed hydrogel network. Upon removal of compression, the fluorescence intensity decreased, confirming the Fc^+-mediated re-oxidation of thiols back to disulfides. The confocal images display fluorescence intensity gradient profiles (Figure 3D), with minimum intensity near the electrode surface (within 400 µm) and maximum intensity on the opposite side. After stress removal, the thickness of the upper fluorescent region decreases (image at 60 min) and nearly disappears following ≈ 180 min of voltage application. This is consistent with the fact that the oxidation of thiols to disulfides initiates at the electrode surface, where Fc^+ is generated and then propagates into the bulk hydrogel along the diffusion path of Fc^+. The hydrogel subjected to 30 min of compression without

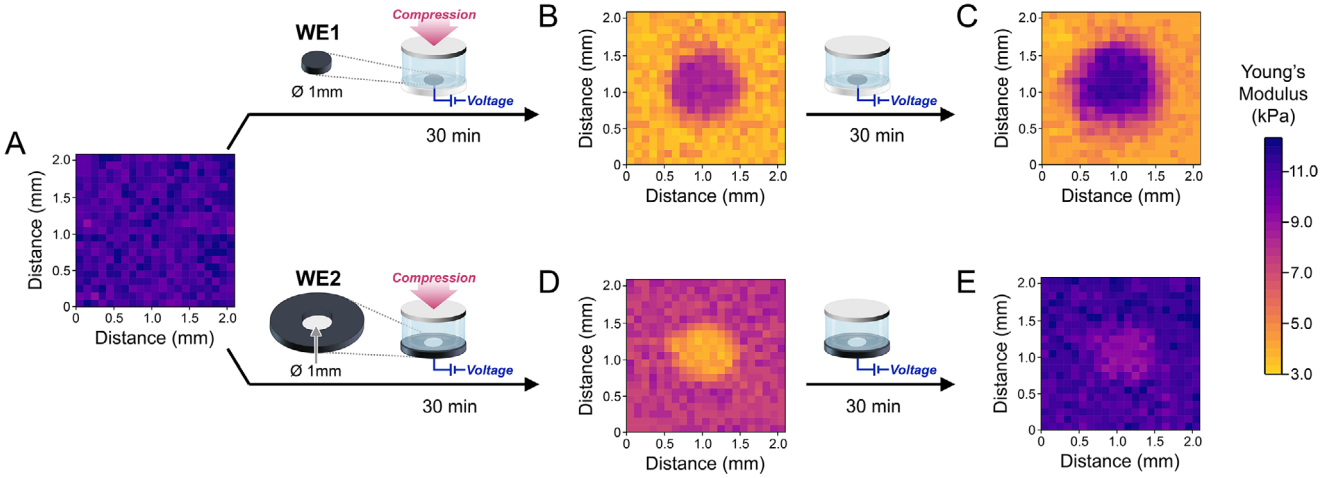

Figure 4. Surface maps of microindentation measurements of A) the as-prepared hydrogel, B,D) hydrogels subjected to 3.9 kPa compression stress for 30 min under continuous application of 1.0 V in 8 mM Fc solution using WE1 (B) or WE2 (D), and C,E) hydrogels following compression removal and an additional 30 min of voltage application using WE1 (C) or WE2 (E).

applied voltage exhibited a homogeneous fluorescence intensity across its thickness (Figure 3E). These results demonstrate that electricity can modulate the response of the hydrogel network, enabling adaptation to various mechanical environments by generating a gradient of thiol conversion, and thus stiffness, across the network in the direction of the electrogenerated oxidant. The interplay between mechanical input and electrochemical oxidation, acting as a feedback, gives rise to spatiotemporal control of hydrogel stiffness under out-of-equilibrium conditions.

2.3. Out-of-Equilibrium Stiffness Patterns

We explored whether applying compressive stress to the hydrogel, combined with the diffusion of oxidant from an electrode with defined shape and size can be used to generate spatial patterns of stiffness on the hydrogel. Indeed, developing hydrogels with stiffness patterns is crucial for many biological applications, especially to mimic native extracellular matrix (ECM) to study cell-behaviors.[5] Spatial modulation of stiffness in hydrogels has been demonstrated to influence cell proliferation or differentiation and thereby control cell phenotype.[23] Photopatterning has been used to generate stiffness patterns of various geometries or gradients on hydrogels.[39,40] However, most patterned hydrogels are static and cannot recapitulate the dynamic properties of natural ECMs, which feature multiple graded stiffness and concentration profiles that evolve over time.

To achieve dissipative stiffness patterning, we used screen-printed electrodes configured with either i) a circular working electrode of 1.0 mm in diameter (WE1), or ii) a ring-shaped working electrode of 4.0 mm in diameter featuring a 1.0 mm diameter non-conductive center (WE2). The local mechanical properties of the hydrogel on the surface in contact with the electrode were probed by microindentation. Surface mapping of the hydrogel before compression revealed a uniform Young's modulus of ≈ 10–12 kPa, with no discernible pattern (**Figure** 4A). This value is consistent with the Young's modulus obtained from the compression test on the bulk hydrogel (Figure 2A). The hydrogel disk was then placed onto the screen-printed electrode, and a weight was applied to the opposite side of the hydrogel disk, resulting in a compressive stress of 3.9 kPa. Simultaneously, a constant voltage of 1.0 V was applied for 30 min at the 1.0 mm WE1.

Microindentation mapping of the hydrogel surface displays two distinct stiffness regions: a central circular area of ≈1 mm diameter with a Young's modulus of ≈6–7 kPa, and an outer region with a Young's modulus of ≈3–4 kPa (Figure 4B). The region exhibiting higher stiffness closely matched the shape and diameter of the WE1. In contrast, the area not in contact with the electrode displayed a Young's modulus comparable to that of the hydrogel subjected to 30 min of compression without applied potential (Figure S6, Supporting Information). After removal of compression from the patterned hydrogel and the application of the voltage for an additional 30 min, microindentation surface mapping revealed an enlargement of the central region, with stiffness increasing to 9–11 kPa (Figure 4C). To further demonstrate the ability of our approach to generate stiffness patterns with high fidelity to the electrode geometry, we employed a screen-printed electrode with a 4.0 mm WE comprising a non-conductive center of 1.0 mm in diameter (WE2). A hydrogel disk was placed on this electrode and subjected to a compressive stress of 3.9 kPa for 30 min, while a continuous voltage of 1.0 V was applied. Microindentation map revealed a well-defined central circular region ≈ 1 mm in diameter with a low Young's modulus of 3–4 kPa, corresponding to the non-conductive center and a surrounding region with a Young's modulus in the range of 7–9 kPa (Figure 4D), corresponding to the area in contact with the working electrode. After the removal of the compressive stress, continuous voltage application for an additional 30 min led to the near disappearance of the patterned stiffness, with the hydrogel recovering a uniform modulus in the original range of 10–12 kPa (Figure 4E). These results indicate that pattern formation occurred under out-of-equilibrium conditions regulated by compression and voltage application.

To further support our conclusion, hydrogels were subjected to compression for 30 min, followed by a separate application of 1.0 V for 30 min using either WE1 or WE2. These conditions

did not provide stiffness patterns matching the shape and size of the electrodes, and broadened high-stiffness regions were observed, likely due to the extended diffusion of Fc^+ generated at the conductive surface (Figure S7, Supporting Information). Therefore, the coupling of force-induced bond cleavage with the electrochemical reoxidation of thiols to disulfides, governed by the diffusion of the redox mediator from the electrode, enables the design of materials with spatiotemporal stiffness control. The stiffness patterns achieved here are on the millimeter scale, but finer feature sizes and more complex geometries could be obtained using electrodes, as well as arrays, of different shapes. Unlike systems operating at equilibrium, where hydrogel stiffness is switched between two states by external stimuli, our approach enables the transient and spatially resolved generation of stiffness patterns within the hydrogel, unlocking new possibilities for advanced bioengineering applications.

2.4. Transient Protein Release Induced by Mechano-Chemical Dissipation

Mechano-responsive biocompatible materials have attracted significant interest for on-demand drug release, as applied forces like compression in skeletal structures and tension in muscles can be harnessed from the physiological environment to activate the release process in situ.[41] Force-induced release of small molecules has been achieved using mechanoresponsive prodrug systems that incorporate mechanochemically labile bonds.[28,42] Therapeutic proteins physically encapsulated in hydrogel matrices have also been released in response to mechanical stimuli.[43] Although these systems enable precise control over release, they are limited by the amount of drug that can be released and the challenge of achieving iterative release, as the matrices often dissociate after the initial mechanical activation. Here, we demonstrate the advantages of force-induced temporal control over hydrogel stiffness for achieving transient, dose-controlled release of payloads, as compared to classical systems that operate under equilibrium conditions.

Considering that H_2O_2 is a byproduct of many enzymatic reactions, and in particular it is produced upon oxidation of glucose (an essential metabolic substrate) by oxygen catalyzed by glucose oxidase (GOx), we designed a system where GOx is entrapped within the hydrogel enabling in situ biocatalytic production of H_2O_2 for the reoxidation of thiols to disulfides upon hydrogel compression. We used fluorescein-labeled bovine serum albumin (FITC-BSA), as a model protein payload. Rheological characterization of the hydrogel loaded with FITC-BSA revealed a storage modulus comparable to that of hydrogel disks without the protein (Figure S8, Supporting Information), indicating that the protein is physically entrapped within the hydrogel network without significantly affecting its mechanical properties. As depicted in **Figure** 5A, the hydrogel loaded with FITC-BSA and GOx is soaked in a glucose solution and subjected to compressive stress. Compression of the protein-loaded hydrogel at 5.9 kPa stress for 30 min in the presence of 20 mM glucose results in a decrease in G' from 290 to 180 Pa (Figure S9, Supporting Information), attributed to compression-induced disulfide bond rupture. Following the release of the compression, the stiffness of the hydrogel gradually recovers, returning to its original value in ≈8 h. In contrast, subjecting the hydrogel to the same compressive stress without glucose results in a drop of G' to a constant value of ≈130 Pa. This result demonstrates that H_2O_2, a by-product of GOx activity, is responsible for mediating thiol re-oxidation to restore the high-stiffness state. At a fixed glucose concentration, the minimum transient stiffness (G'_{min}) decreases with the level of applied compression (Figure 5B), and the lifetime of the softened hydrogel increases from 3.5 h under 2.0 kPa to 6 h under 3.9 kPa. The G'_{min} values can be tuned by adjusting the glucose concentration at constant stress. As glucose concentration increases, G'_{min} progressively rises (Figure S9B, Supporting Information) due to the higher levels of H_2O_2 generated by the GOx-catalyzed reaction. Control experiments revealed no change in hydrogel stiffness in the presence of 20 mM glucose when the hydrogel was not subjected to compression. The transient softening of the hydrogel under compression in the presence of glucose allowed us to employ the protein-loaded hydrogel as a platform for releasing FITC-BSA, induced by compression. Figure 5C shows the time-dependent release profiles of FITC-BSA from the hydrogel, monitored using fluorescence spectroscopy. In the absence of compression, the fully crosslinked hydrogel effectively prevents any leakage of FITC-BSA (Figure 5C, gray curve). By contrast, applying compressive stress of 5.9 kPa for 30 min induces a rapid protein release, reaching near-complete release (91 ± 4%) within ≈7 h. In the presence of 20 mM glucose, the FITC-BSA release from the hydrogel under the same compressive stress is slower, reaching a plateau of ≈70 ± 3% over 6 h. The lower release compared to that observed without glucose is due to the concurrent re-oxidation of thiols mediated by H_2O_2, a by-product of GOx activity, which restores disulfide crosslinking and blocks the FITC-BSA release from the hydrogel. Reducing the compressive stress in the presence of glucose from 5.9 to 2.0 kPa decreases the release kinetics, and the amount of FITC-BSA released at the plateau also decreases. This is consistent with the shorter lifetimes of the transient softening observed under lower compressive stress, allowing the hydrogel to return to a fully cross-linked state more quickly, thereby blocking further protein release.

Having established a dose-controlled release under dissipative conditions, we turn to the challenge of achieving iterative protein release through multiple applications of compressive stress to the hydrogel. In the presence of 20 mM glucose, the hydrogel was subjected to cycles of 2.0 kPa compressive stress for 30 min, alternating with 30 min intervals of compression release. Each compression cycle of the hydrogel induces the release of ≈ 6%–7% of FITC-BSA, resulting from disulfide bond rupture and network weakening (Figure 5D). After each compression removal, the H_2O_2 produced by GOx restores the disulfide crosslinkers within the hydrogel, thus blocking the release of FITC-BSA. Next, we investigated the temporal and spatial control of load release from the hydrogel by applying compression with a Teflon mold featuring 2.0 mm diameter holes. The FITC-BSA-loaded hydrogel, initially showing uniform fluorescence as observed by fluorescence microscopy (Figure 5E), was subjected to 5.9 kPa compressive stress for 30 min using the Teflon mold in the presence of 20 mM glucose. After compression removal, a distinct pattern persists on the hydrogel, featuring green, fluorescent circles ≈ 2 mm in diameter corresponding to the mold holes; there FITC-BSA remains entrapped within the network. These circles are surrounded by darker regions that experienced compressive

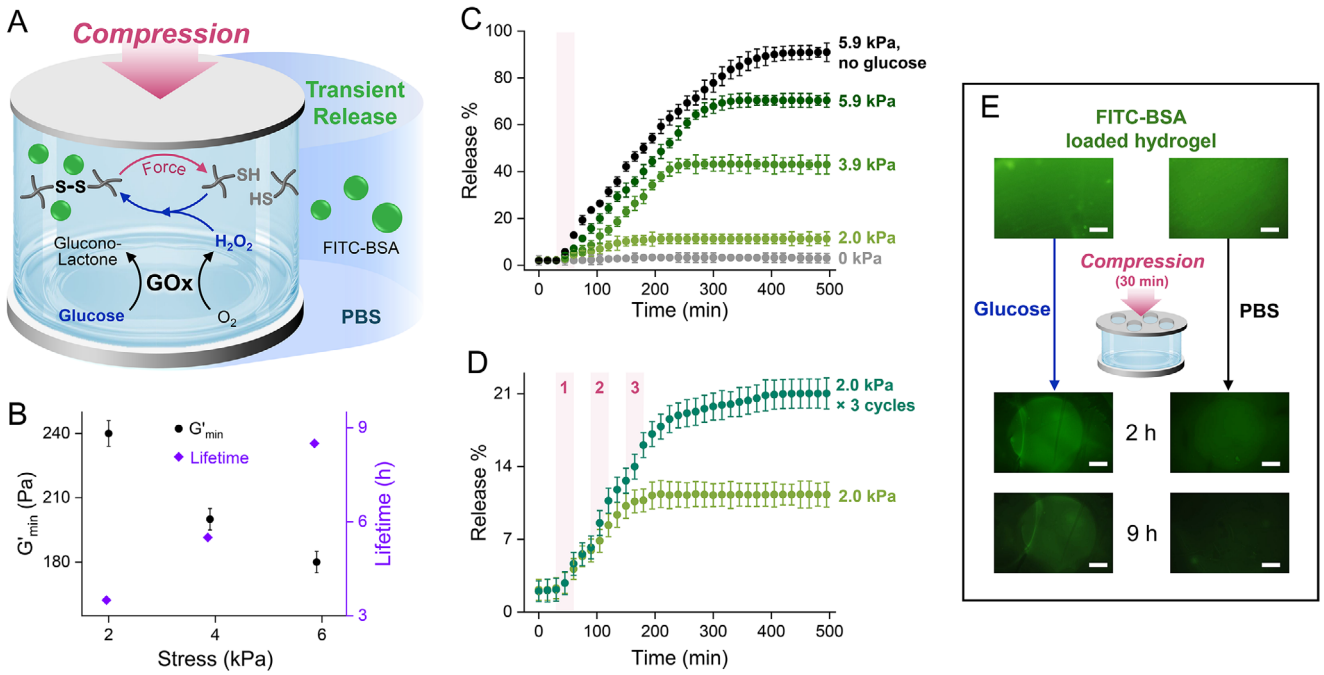

Figure 5. Transient protein release under compressive stress and enzymatic feedback. A) Schematic representation of temporal weakening in a FITC-BSA and GOx-loaded hydrogel, triggered by compressive stress and regulated by H_2O_2 generated from GOx in the presence of glucose, leading to transient FITC-BSA release. B) Minimum stiffness (G'_{min}) and lifetimes of the GOx-loaded hydrogel subjected to different compressive stress for 30 min in the presence of 10 mM glucose in PBS 0.1 M at pH 7.4. C) Time-dependent release of FITC-BSA from hydrogels in a 20 mM glucose solution subjected to 30 min compressive stresses (kPa): 0, 2.0, 3.9 and 5.9. Black curve represents the release profile from the hydrogel subjected to 5.9 kPa compressive stress for 30 min without glucose. D) Time-dependent release of FITC-BSA from hydrogels in a 20 mM glucose solution subjected to single (light green) and multiple (dark green) 2.0 kPa compressive stresses, each applied for 30 min and alternated with intervals of 30 min of compression removal. E) Fluorescence microscopy images collected on the hydrogel loaded with FITC-BSA and after application of 5.9 kPa for 30 min using a mold with 2 mm holes in the presence of 20 mM glucose (left) and in PBS solution (right). Scale bar 0.5 mm.

stress, where FITC-BSA was released. The amount of FITC-BSA released into the solution was estimated to be ≈ 63% (Figure S10, Supporting Information). In contrast, in the absence of glucose, the green, fluorescent circles resulting from the compression with the mold fade within 2 h after compression release and disappear completely after 9 h, with fluorescence entirely lost from the hydrogel and almost complete release (95%) of FITC-BSA into the solution. The pattern fidelity observed on the hydrogel in the presence of glucose is attributed to H_2O_2 enzymatically produced in situ, which restores the disulfide-crosslinked network and prevents protein leakage from the non-compressed regions. In contrast, without glucose, the pattern is not maintained as FITC-BSA gradually leaks from the non-compressed regions and is released from the softened hydrogel. These results demonstrate the advantages of our approach of force-induced, temporally controlled modulation of hydrogel stiffness to achieve transient, dose-controlled protein release.

3. Conclusion

Biological systems harness mechano-chemical dissipative processes to relieve mechanical stress, with chemical and mechanical responses continuously adjusting to each other. We have demonstrated that a mechano-responsive hydrogel can achieve temporal modulation of its stiffness as an adaptive response to force-driven deformation. This response is managed by chemical or electrochemical-generated oxidants, which drive crosslinking reactions within the hydrogel network, enabling precise control over its transient stiffness properties. The use of electrochemically generated oxidants as feedback for mechanical stress provides high spatiotemporal control and enables the direction of the dissipative process in a more complex fashion. By leveraging the gradient of electrogenerated oxidants diffusing from the electrode into the hydrogel under compressive stress, we created temporal stiffness patterns within the material. In general, diffusion-dependent out-of-equilibrium patterns play central roles in complex spatial self-organization, including embryogenesis.[44] We believe that electrically regulated dissipative processes driven by a mechanical energy input, that we developed here, provide a framework for the rational engineering of functional out-of-equilibrium materials. To further showcase the versatility of our approach, we have applied the out-of-equilibrium modulation of the hydrogel stiffness, regulated by mechanical stress and localized generation of oxidants via enzymatic reactions, for the transient release of protein payloads.

The concepts presented in this work offer new perspectives for the development of adaptive and self-regulating materials that couple mechanical and electrochemical processes, where mechanical inputs modulate chemical transformations, and electrochemical oxidation in turn controls the material's mechanical properties. Such transient, force-responsive materials hold strong potential for soft robotics, enabling self-regulating

stiffness, energy dissipation, and sensing functionalities. When integrated with embedded electrodes or flexible electronics, this approach could drive the development of untethered, reconfigurable actuators and bio-integrated systems with sustained mechanical adaptability.[45] These advancements can pave the way for developing next-generation autonomous biomedical devices[46,47] and interactive human-machine interfaces,[48] mimicking complex mechanotransduction processes.

4. Experimental Section

Materials: All reagents were purchased from commercial suppliers and used without further purification. Four-arm thiol-terminated poly(ethylene glycol) (4-arm-PEG-SH, MW 5000) was purchased from JenKem Technology USA (Plano, TX). Iron(III) nitrate nonahydrate ($Fe(NO_3)_3{\cdot}9H_2O$; 98%), ethylenediaminetetraacetic acid disodium salt dihydrate (EDTA; 99%), 30% (w/w) hydrogen peroxide (H_2O_2) solution, D-glucose (99.5%), 2,2′-azinobis(3-ethylbenzothiazolinesulfonic acid) diammonium salt (ABTS; 98%), ferrocenecarboxylic acid (Fc, >97%), glucose oxidase from Aspergillus niger (GOx; 145 U mg^{-1}), horseradish peroxidase (HRP; 200 U mg^{-1}), sodium phosphate monobasic dihydrate (>99.0%), sodium phosphate dibasic dihydrate (>99.0%), fluorescein isothiocyanate (FITC, >90%), and FITC conjugated with bovine serum albumin (FITC-BSA) were all purchased from Sigma–Aldrich Co (St. Louis, MO).

Instrumentation: Rheological characterizations were performed on a Kinexus Lab+ rheometer (Malvern Instruments, UK) with a 20 mm plate geometry at a fixed gap. Compression tests were performed at room temperature using a mechanical analyzer (DMA Q800, TA Instrument). Cylindrical gel disks with a diameter of 9 mm and height of 2 mm were placed between two clamps and compressed at 10% strain per min until failure. The local mechanical properties of patterned hydrogels were assessed using a Piuma Nanoindenter (Optics 11, Amsterdam, NL) equipped with a spherical probe with a radius of 23 µm and a cantilever with a stiffness of 0.55 N m^{-1}. The grid scan was 20 × 20 points, and the point-to-point pitch was 100 µm. The effective Young's modulus was calculated using the Oliver and Pharr model. Electrochemical experiments were performed with a potentiostat/galvanostat PGSTAT204 (Metrohm Autolab B.V.) using screen-printed electrodes (Metrohm-Dropsens, Oviedo, ES), comprising a glassy carbon working electrode, an Ag/AgCl reference electrode and a carbon counter electrode. Fluorescence spectra were collected on FLS1000 fluorimeter by Edinburgh Instruments, using a quartz cuvette of 1 cm path length (bandwidth: 1.0 nm; emission bandwidth: 1.0 nm). Confocal laser microscopy was performed on a Zeiss LSM 900 with Airyscan 2 equipped with Zeiss EC Plan–Neofluar 10x/0.5 objective employing an excitation wavelength of 488 nm. The images were processed using the Zeiss ZEN and ImageJ software. Fluorescence images of the hydrogel films loaded with FITC-BSA were acquired with an upright Leica DM6 optical microscope. Ultraviolet-visible (UV–vis) spectra were collected using an Agilent Cary 60 spectrophotometer.

Preparation of 4-arm-PEG Hydrogels: Hydrogel disks were prepared in a cylindrical plastic mold (diameter: 9 mm), following a reported procedure with some modifications.[30] Briefly, a solution (85 µl) of Fe^{3+} (200 mM) and EDTA (200 mM) in 0.1 M phosphate-buffered saline (PBS), pH 7.4, was added to a 10% w/v solution of a 4-arm-PEG-SH (85 µl) in PBS 0.1 M at pH 7.4. The resulting solution was incubated at 34 °C in a humidified environment for 1 h. The obtained hydrogels were removed from the mold and washed in DI water for 2 h prior to use. For the electrochemical experiments, hydrogel disks were prepared in plastic molds with a diameter of 4 mm, and the procedure was scaled accordingly.

Preparation of Protein-Loaded Hydrogels: Hydrogel disks loaded with GOx and FITC-BSA for the release experiments were prepared following the procedure described in the previous paragraph, with slight modifications. A solution (85 µl) of Fe^{3+} (200 mM) and EDTA (200 mM) in 0.1 M PBS, pH 7.4, was added to a 10% w/v solution of a 4-arm-PEG-SH (85 µl) comprising GOx (5 mg ml^{-1}) and FITC-BSA (3 mg ml^{-1}) in PBS 0.1 M at pH 7.4, and was incubated at 34 °C in a humidified environment for 1 h. The hydrogels were removed from the mold and immersed in DI water for 5 h prior to use to remove any adsorbed proteins.

Characterization of Hydrogels by Confocal Laser Microscopy: To monitor the cleavage of the disulfide crosslinked hydrogels following the application of compressive stress, the polymer disks were rinsed with water and then immersed in a 30 µM FITC solution for 30 min. The hydrogels were then soaked in degassed DI water for 1.5 h to remove the unreacted FITC. Confocal images were collected using an excitation wavelength of 488 nm on the z-direction perpendicular to the hydrogel disk. The average fluorescence intensity of each frame of the hydrogel was extracted, and the average fluorescence intensity of all frames was determined.

Glucose Oxidase Activity Assay: The activity of the GOx embedded into the hydrogel network was quantified using an ABTS-HRP coupled assay, following a previously reported procedure with some modifications.[49] The protein-loaded hydrogel disk was immersed into a PBS solution (1.5 ml; 0.1 M, pH 7.4) containing HRP (3 U), ABTS (3 mg), and D-glucose (10 mM). The UV–vis spectrum of the solution collected after 30 s was measured to determine enzyme activity. One unit of activity is defined as the amount of GOx that is able to produce 1 µmol product per min under the reaction conditions. After the hydrogel preparation, the catalytically active GOx units entrapped in the hydrogel network are 2.1 ± 0.1 U gel^{-1}.

Mechano-Chemical Dissipative Experiments: Hydrogel disks were equilibrated for 15 min in 3 ml solution of 0.1 M PBS pH 7.4 in the presence of 10 mM H_2O_2. Hydrogels were subsequently subjected to different compressive stresses (2.0, 3.9, and 5.9 kPa) for 1 h in this solution, after which the compressive stress was removed. The mechanical properties of the hydrogels were assessed at various time intervals using a rheometer with a temperature-controlled parallel plate configuration (20 mm diameter steel plates). Measurements were conducted at a temperature of 25 °C, in fixed-gap mode, at a frequency of 1 Hz and 0.1% strain. To assess the effect of H_2O_2 concentration on rheological properties, hydrogel disks were equilibrated for 15 min in a 3 ml solution of 0.1 M PBS pH 7.4 with increasing H_2O_2 concentrations (2.5, 10, and 25 mM), followed by the application of a 3.9 kPa compressive stress for 1 h.

Mechano-Electrochemical Dissipative Experiments: Hydrogel disks were immersed in an 8 mM Fc solution in 0.1 M PBS pH 7.4 for 30 min before being transferred onto the surface of the screen-printed electrode. An 8 mM Fc solution in 0.1 M PBS pH 7.4 (500 µl) was added and a constant voltage of 1.0 V was applied. After 10 min, the hydrogel disks were subjected to different compressive stresses (2.0, 3.9, and 5.9 kPa) for 30 min while a continuous voltage was applied. The mechanical properties of the hydrogels were evaluated at different time intervals using a rheometer with a temperature-controlled parallel plate configuration (20 mm diameter steel plates). Measurements were conducted at a temperature of 25 °C, in fixed-gap mode, at a frequency of 1 Hz and 0.1% strain.

For the patterning experiments, hydrogel disks were placed onto the surface of a screen-printed electrode featuring a circular glassy carbon working electrode (WE1: 1.0 mm diameter) or a ring-shaped configuration (WE2: 4.0 mm outer diameter with a 1.0 mm diameter non-conductive center). An 8 mM Fc solution in 0.1 M PBS pH 7.4 (500 µl) was added to cover the hydrogel. A constant voltage of 1.0 V was then applied to the working electrode for 30 min while simultaneously applying a compressive stress of 3.9 kPa to the hydrogel. Following the removal of the compressive stress, the voltage was maintained for an additional 30 min. The stiffness of the hydrogel region in contact with the screen-printed electrode was assessed by indentation measurements.

Mechano-Enzymatic Dissipative Experiments: For the enzymatic driven dissipative experiments, protein-loaded hydrogel disks were equilibrated for 1 h in 2 ml solution of 0.1 M PBS pH 7.4 in the presence of 20 mM glucose. Subsequently, hydrogels were subjected to different compressive stresses (2.0, 3.9 and 5.9 kPa) for 30 min in the glucose solution, after which the compressive stress was removed. The stiffness of the hydrogels was evaluated at different time intervals using a rheometer, in fixed-gap mode, at a frequency of 1 Hz and 0.1% strain. The stiffness of the hydrogels was also evaluated after a 1 h equilibration in 2 ml of 0.1 M PBS (pH 7.4)

containing increasing glucose concentrations (0, 1, 5, 10, 20, and 30 mM) and following the application of a 3.9 kPa compressive stress for 30 min.

FITC-BSA Release Study: For monitoring the release of FITC-BSA from the hydrogel, protein-loaded hydrogel disks were placed in 2 ml of 0.1 M PBS solution (pH 7.4), in the presence of 20 mM glucose, and subjected to different compressive stresses (2.0, 3.9, and 5.9 kPa) for 30 min. The release of the FITC-BSA was monitored by fluorescence spectroscopy (λ_{ex} = 482 nm; λ_{em} = 520 nm) collecting the fluorescence intensities at time intervals of 15 min during the course of the experiment. FITC-BSA released from the hydrogel was quantified using a calibration curve generated with solutions of FITC-BSA from 1 to 60 µg ml^{-1} in PBS 0.1 M at pH 7.4. The maximum amount of FITC-BSA that could be released from the protein-loaded hydrogels was determined by measuring the FITC-BSA released after 1 day from the application of the 5.9 kPa compressive stress on the hydrogel equilibrated in PBS solution. The release percentage was calculated from the maximum amount of FITC-BSA from the hydrogel and the amount of FITC-BSA released under the different conditions.

For release experiments under multiple compressive stresses, the hydrogels were placed in 2 ml of 0.1 M PBS (pH 7.4) in the presence of 20 mM glucose and subjected to repeated cycles of 2.0 kPa compressive stress for 30 min, alternating with 30 min without compression. For patterned release experiments, the hydrogels were placed in 2 ml of 0.1 M PBS (pH 7.4) in the presence of 20 mM glucose and subjected to a compressive stress of 5.9 kPa for 30 min. A Teflon mold (10 mm in diameter) with circular holes of 2.0 mm in diameter was used to pattern the protein release from the hydrogel.

Supporting Information

Supporting Information is available from the Wiley Online Library or from the author.

Acknowledgements

This research was supported by Next Generation EU PRIN 2022 (M4.C2.1.1) under the Prot. 2022WN89PC and by Cariparo Foundation with the framework of the project "NoneQ" (PRIN_CARIVARI24_01).

Open access publishing facilitated by Universita degli Studi di Padova, as part of the Wiley - CRUI-CARE agreement.

Conflict of Interest

The authors declare no conflict of interest.

Data Availability Statement

The data that support the findings of this study are available from the corresponding author upon reasonable request.

Keywords

adaptive materials, drug delivery, electrochemistry, hydrogels, mechanochemistry, non-equilibrium processes

Received: January 25, 2025
Revised: April 12, 2025
Published online:

[1] M. M. Lerch, A. Grinthal, J. Aizenberg, *Adv. Mater.* **2020**, *32*, 1905554.
[2] M. A. Kostiainen, A. Priimagi, J. V. I. Timonen, R. H. A. Ras, M. Sammalkorpi, M. Penttilä, O. Ikkala, M. B. Linder, *Adv. Funct. Mater.* **2024**, *34*, 2402097.
[3] M. Chalfie, *Nat. Rev. Mol. Cell Biol.* **2009**, *10*, 44.
[4] A. M. Rosales, K. S. Anseth, *Nat. Rev. Mater.* **2016**, *1*, 15012.
[5] A. Bailles, E. W. Gehrels, T. Lecuit, *Annu. Rev. Cell Dev. Biol.* **2022**, *38*, 321.
[6] S. A. P. van Rossum, M. Tena-Solsona, J. H. van Esch, R. Eelkema, J. Boekhoven, *Chem. Soc. Rev.* **2017**, *46*, 5519.
[7] S. De, R. Klajn, *Adv. Mater.* **2018**, *30*, 1706750.
[8] K. Das, L. Gabrielli, L. J. Prins, *Angew. Chem., Int. Ed.* **2021**, *60*, 20120.
[9] C. W. H. Rajawasam, C. Tran, M. Weeks, K. S. McCoy, R. Ross-Shannon, O. J. Dodo, J. L. Sparks, C. S. Hartley, D. Konkolewicz, *J. Am. Chem. Soc.* **2023**, *145*, 5553.
[10] X. He, M. Aizenberg, O. Kuksenok, L. D. Zarzar, A. Shastri, A. C. Balazs, J. Aizenberg, *Nature* **2012**, *487*, 214.
[11] L. Heinen, T. Heuser, A. Steinschulte, A. Walther, *Nano Lett.* **2017**, *17*, 4989.
[12] M. Jain, B. J. Ravoo, *Angew. Chem., Int. Ed.* **2021**, *60*, 21062.
[13] R. Baretta, M. Frasconi, *J. Am. Chem. Soc.* **2024**, *146*, 7408.
[14] H. Zhang, H. Zeng, A. Eklund, H. Guo, A. Priimagi, O. Ikkala, *Nat. Nanotechnol.* **2022**, *17*, 1303.
[15] C. Li, A. Iscen, H. Sai, K. Sato, N. A. Sather, S. M. Chin, Z. Álvarez, L. C. Palmer, G. C. Schatz, S. I. Stupp, *Nat. Mater.* **2020**, *19*, 900.
[16] X. Yang, W. Shi, Z. Chen, M. Du, S. Xiao, S. Qu, C. Li, *Adv. Funct. Mater.* **2023**, *33*, 2214394.
[17] G. Fusi, D. Del Giudice, O. Skarsetz, S. Di Stefano, A. Walther, *Adv. Mater.* **2023**, *35*, 2209870.
[18] R. Baretta, G. Davidson-Rozenfeld, V. Gutkin, M. Frasconi, I. Willner, *J. Am. Chem. Soc.* **2024**, *146*, 9957.
[19] J. Li, C. Nagamani, J. S. Moore, *Acc. Chem. Res.* **2015**, *48*, 2181.
[20] G. De Bo, *Chem. Sci.* **2018**, *9*, 15.
[21] T. Matsuda, R. Kawakami, R. Namba, T. Nakajima, J. P. Gong, *Science* **2019**, *363*, 504.
[22] K. Seshimo, H. Sakai, T. Watabe, D. Aoki, H. Sugita, K. Mikami, Y. Mao, A. Ishigami, S. Nishitsuji, T. Kurose, H. Ito, H. Otsuka, *Angew. Chem., Int. Ed.* **2021**, *60*, 8406.
[23] N. Gjorevski, M. Nikolaev, T. E. Brown, O. Mitrofanova, N. Brandenberg, F. W. DelRio, F. M. Yavitt, P. Liberali, K. S. Anseth, M. P. Lutolf, *Science* **2022**, *375*, aaw9021.
[24] S. Palagi, P. Fischer, *Nat. Rev. Mater.* **2018**, *3*, 113.
[25] A. P. Wiita, S. R. K. Ainavarapu, H. H. Huang, J. M. Fernandez, *Proc. Natl Acad. Sci. USA* **2006**, *103*, 7222.
[26] D. Xu, M. Wang, R. Huang, J. F. Stoddart, Y. Wang, *J. Am. Chem. Soc.* **2025**, *147*, 4450.
[27] K. R. Fitch, A. P. Goodwin, *Chem. Mater.* **2014**, *26*, 6771.
[28] Z. Shi, J. Wu, Q. Song, R. Göstl, A. Herrmann, *J. Am. Chem. Soc.* **2020**, *142*, 14725.
[29] M. Xuan, J. Fan, V. N. Khiêm, M. Zou, K.-O. Brenske, A. Mourran, R. Vinokur, L. Zheng, M. Itskov, R. Göstl, A. Herrmann, *Adv. Mater.* **2023**, *35*, 2305130.
[30] C.-Y. Lin, C. M. Battistoni, J. C. Liu, *Biomacromolecules* **2021**, *22*, 5270.
[31] A. F. Wilderspin, N. M. Green, *Anal. Biochem.* **1983**, *132*, 449.
[32] V. Schnaible, M. Przybylski, *Bioconjugate Chem.* **1999**, *10*, 861.
[33] G. L. Grocke, H. Zhang, S. S. Kopfinger, S. N. Patel, S. J. Rowan, *ACS Macro Lett.* **2021**, *10*, 1637.
[34] G. Ragazzon, M. Malferrari, A. Arduini, A. Secchi, S. Rapino, S. Silvi, A. Credi, *Angew. Chem., Int. Ed.* **2023**, *62*, 202214265.
[35] D. Barpuzary, P. J. Hurst, J. P. Patterson, Z. Guan, *J. Am. Chem. Soc.* **2023**, *145*, 3727.
[36] A. J. Bard, L. R. Faulkner, *Electrochemical Methods: Fundamentals and Applications*, John Wiley & Sons, New York, **2001**.
[37] C. Yang, Y. Liu, M. Wang, H. Hu, Z. Zhao, H. Deng, G. F. Payne, X. Shi, *Adv. Funct. Mater.* **2023**, *33*, 2302549.

[38] Y. Li, C. Yang, F. Hu, H. Hu, Y. Xu, H. Deng, Y. Du, X. Shi, *ACS Appl. Mater. Interfaces* **2024**, *16*, 21463.
[39] R. G. Wylie, S. Ahsan, Y. Aizawa, K. L. Maxwell, C. M. Morshead, M. S. Shoichet, *Nat. Mater.* **2011**, *10*, 799.
[40] L. Li, J. M. Scheiger, P. A. Levkin, *Adv. Mater.* **2019**, *31*, 1807333.
[41] Z. Shi, Y. Hu, X. Li, *J. Controlled Release* **2024**, *365*, 259.
[42] L. Chen, R. Nixon, G. De Bo, *Nature* **2024**, *628*, 320.
[43] S. Bianco, M. Hasan, A. Ahmad, S.-J. Richards, B. Dietrich, M. Wallace, Q. Tang, A. J. Smith, M. I. Gibson, D. J. Adams, *Nature* **2024**, *631*, 544.
[44] M. Valet, E. D. Siggia, A. H. Brivanlou, *Nat. Rev. Mol. Cell Biol.* **2022**, *23*, 169.
[45] S. I. Rich, R. J. Wood, C. Majidi, *Nat. Electron.* **2018**, *1*, 102.
[46] S. M. Mirvakili, R. Langer, *Nat. Electron.* **2021**, *4*, 464.
[47] Y. Wang, Z. Chen, B. Davis, W. Lipman, S. Xing, L. Zhang, T. Wang, P. Hafiz, W. Xie, Z. Yan, Z. Huang, J. Song, W. Bai, *Nat. Commun.* **2024**, *15*, 511.
[48] W. Wang, Y. Jiang, D. Zhong, Z. Zhang, S. Choudhury, J.-C. Lai, H. Gong, S. Niu, X. Yan, Y. Zheng, C.-C. Shih, R. Ning, Q. Lin, D. Li, Y.-H. Kim, J. Kim, Y.-X. Wang, C. Zhao, C. Xu, X. Ji, Y. Nishio, H. Lyu, J. B.-H. Tok, Z. Bao, *Science* **2023**, *380*, 735.
[49] L. Sun, T. Bulter, M. Alcalde, I. P. Petrounia, F. H. Arnold, *ChemBioChem* **2022**, *3*, 781.